RSC Advances

PAPER

View Article Online
View Journal | View Issue

Cite this: *RSC Adv.*, 2016, **6**, 5881

MOF–polymer enhanced compatibility: post-annealed zeolite imidazolate framework membranes inside polyimide hollow fibers†

Fernando Cacho-Bailo,[a] Guillermo Caro,[a] Miren Etxeberría-Benavides,[b] Oğuz Karvan,[b] Carlos Téllez[a] and Joaquín Coronas*[a]

Received 7th December 2015
Accepted 29th December 2015

DOI: 10.1039/c5ra26076k

www.rsc.org/advances

Thermal annealing, a commonly used procedure for improving the performance of polymeric membranes, is in this work exploited in the presence of a metal–organic framework (MOF) supported layer. MOFs and polymers are materials with a common organic character, suggesting an enhanced affinity between them when used together in membrane separation. Zeolite-like imidazolate frameworks (ZIFs) ZIF-8 and ZIF-93 with sod and rho structures and pore apertures of 0.34 and 0.36 nm, respectively, have been grown inside 356 μm OD co-polyimide P84 hollow fibers by microfluidics, leading to continuous supported membranes. When these membranes were thermally *in situ* annealed below the glass transition temperature, while monitoring both H_2 and CH_4 permeances, the MOF–polymer adhesion was enhanced. Thus the gas separation selectivity increased without any significant reduction in the gas permeance, and H_2/CH_4 and CO_2/CH_4 maximum selectivities of 103 and 18 (ZIF-8) and 101 and 20 (ZIF-93) were respectively measured. The good compatibility between MOF and polymer made improvements possible in the annealing of the membrane once it was prepared. If the annealing of the polymer was carried out before the MOF synthesis, the polymer chain rearrangement and surface smoothing prevented an optimum MOF–polymer interaction and the separation performance worsened. These results proved the compatibility between both materials and their synergistic contribution to gas selective transport.

Introduction

High-efficiency technologies are required nowadays for the purification of gas streams: CO_2 removal from natural or flue gas and high purity H_2 flows for feeding portable hydrogen batteries are of great concern. Membrane-based processes are attractive for this purpose in terms of economy and environmental friendliness compared with the well-established traditional technologies.[1–3] Polymers shaped as hollow fibers (HFs) are the most efficient alternative for industrial-scale gas separation using membranes. The HF shape maximizes the process efficiency, providing thousands of square meters of permeable area with an improved mass transfer per cubic meter.[4,5] In fact, HFs are widely applied in processes such as reverse osmosis, dialysis,[6] the removal of pollutants from drinking water,[7] *etc.*

Polyimides are one of the most attractive and versatile polymers for the fabrication of high performance membranes to be used in either gas or liquid phase applications.[8] Aromatic polymers (including commercial Matrimid,[9,10] P84, Ultem[11] or Kapton[12]) provide high thermal, physical and chemical stability, most of them having high glass transition temperatures and withstanding organic solvents and weak acids. In particular, P84 (BTDA-TDI/MDI, 3,3′4,4′-benzophenone tetracarboxylic dianhydride, 80% methylphenylene-diamine + 20% methylene diamine) is a noteworthy co-polyimide already applied as a membrane material in gas separation,[13] ultra and nanofiltration[14] and pervaporation.[15,16]

Some of the more common challenges to be overcome by membrane technology, including polyimide based materials, are the permeability/selectivity membrane trade-off related to low productivity, as well as the worsening in the separation performance due to aging or plasticization. Some techniques such as chemical cross-linking or thermal annealing have been widely applied to these polymeric materials to induce chemical or physical changes that lead to enhancements in either their permeability or their aging and plasticization resistance.[8,17,18]

Thermal annealing below the glass transition temperature appears to lead to mere physical and morphological changes in the P84 material,[15,19] whereas some induced cross-linking in

[a]*Chemical and Environmental Engineering Department and Instituto de Nanociencia de Aragón (INA), Universidad de Zaragoza, 50018 Zaragoza, Spain. E-mail: coronas@unizar.es*

[b]*Tecnalia Research and Innovation, Energy and Environmental Division, 20009 Donostia-San Sebastián, Spain*

† Electronic supplementary information (ESI) available: Synthesis parameters of polymeric hollow fibers, ZIF-93@P84 performance dependence during annealing, characterization by XRD, FTIR, TGA, XPS and DSC and extended data of the membrane comparison. See DOI: 10.1039/c5ra26076k

6FDA-based polyimides are reported.[20,21] High-temperature annealing allows the polymeric chains to relocate and reduce their cumulative stress, producing some kind of pore collapse and densification, surface smoothing and a lowering in the void fraction of the material.[19,22] Some authors relate this behavior with the formation of charge-transfer complexes (or CTCs) between nearby electron donor (imide) and acceptor (paraffin) groups in the aromatic polyimide.[23,24] When annealing P84, lower permeabilities with enhanced size and shape molecular discrimination are typically obtained,[25] being the resultant material also more resistant to plasticization at high CO_2 feed pressures, which can be related with the improved rigidity of the polymeric chains and the decrease in the free volume.[20,26,27]

The effect of MOFs on polymers by way of MMMs (mixed-matrix membranes) or supported membranes has been largely studied, since their common organic moieties and their semi-rigid structures predict an enhanced synergy between them.[14,28–31] The MOF crystalline microstructures with tunable pore sizes can help polymer materials to overcome the trade-off regarding high separation selectivities.[32] Although the MOF–polymer interaction understanding is still a remaining challenge,[33] an enough stability of the MOF material forming part of a membrane is expected when submitted to a thermal annealing treatment.

In this work, P84 HF membranes with inner-supported layers of zeolitic imidazolate framework (ZIF-8, Zn(2-*N*-methylimidazole)$_2$) were synthetized by means of microfluidics and then post-annealed. The monitoring of the annealing treatment of a polymer membrane in the presence of a MOF supported layer showed an enhanced compatibility of the materials leading to an important improvement in the membrane separation performance without inducing any damage. Several MOF and specifically ZIF-supported membranes using polymeric HFs as supports have been previously reported.[34–38] Microfluidic setups has been recently applied for inner-supported HF membrane fabrication,[39,40] involving some advantages such as the protection of the MOF layer and an ecofriendly reagent and solvent saving.[39] ZIF-93 (Zn(4-methyl-5-imidazolecarboxaldehyde)$_2$),[41–43] a rho-type aldehyde-functionalized imidazolate framework, was also grown and used to validate the post-annealing strategy carried out with ZIF-8.[44] Even though there have been several reports dealing with MOF@HF membranes,[34–40,44] this is the first time that an annealing thermal treatment has been applied on a MOF-coated polymeric membrane to enhance its permselective properties.

Experimental section

Microfluidic membrane fabrication – ZIF-8 & ZIF-93 crystallization

The MOF-supported membranes were fabricated in a microfluidic system consisting of three syringe pumps (NE-300, New Era Pump Systems) for the reagent solutions and the solvent. These solutions were stored in 20–30 mL polypropylene syringes, as explained in our previous work (see Fig. 1).[39] The solutions were pumped through PTFE tubing (0.04 in ID, 1/16 in OD) and then, just after the mixing of the reagents, into a 20 cm long co-polyimide P84 HF (202 μm ID, 356 μm OD). A PTFE-special glue (Ceys®) was used to seal the membrane to the PTFE tube. Experimental details and parameters about P84 HF fabrication procedure can be found in the ESI and elsewhere.†[11,45]

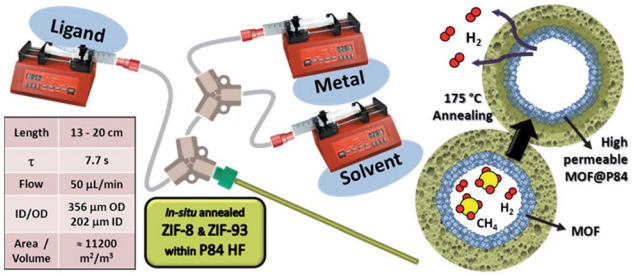

Fig. 1 Experimental microfluidic setup for the fabrication of ZIF-93 and ZIF-8 membranes, including some working parameters and their diagrammatic application in gas separation.

For the fabrication of the ZIF membranes (ZIF-8@P84 and ZIF-93@P84, these meaning the MOF supported on the inner surface of a P84 HF), the P84 HF was first washed with 2 mL of distilled water at 50 μL min^{-1}. Then the metal and ligand clear solutions were pumped in the lumen of the HF support at 25 μL min^{-1} each. Experimental details can be found in our previously reported works[39,44] and in the ESI.† The solution leaving the microfluidic system was collected, centrifuged at 10 000 rpm for 15 min and dried at 100 °C overnight. The collected powders were used for characterization (see Fig. S1,† showing XRD and FTIR spectra), while the fabricated membranes were dried at room temperature overnight.

Membrane and support annealing

Annealing treatments were applied to the fabricated MOF (ZIF-8 and ZIF-93) membranes. They were carried out at 175 °C for 24 h with slow 25 °C h^{-1} rates of heating and cooling (6 h each plus 12 h plateau at maximum temperature), either in a vacuum oven (Memmert VO200) at 10 mbar or *in situ* with a H_2/CH_4/Ar atmosphere while testing in the permeation plant. Furthermore, bare P84 HF supports were also annealed and then used as membrane supports for ZIF-8 and ZIF-93 MOF growth.

Permeation testing and characterization

As-synthesized, vacuum and *in situ* annealed MOF membranes as well as the pure P84 supports were tested in gas separations at 35 °C. Equimolar H_2/CH_4 or CO_2/CH_4 10 cm^3 (STP) min^{-1} mixtures were fed inside the HF membrane lumen. Sweep Ar (H_2/CH_4) or He (CO_2/CH_4) from 1 to 20 cm^3 (STP) min^{-1} streams created a driving force for the gases to permeate through the membranes.

The permeate flows were then analyzed in a micro-gas chromatograph (Agilent 3000A). A total pressure of 1.25 bar was applied on both sides of the membrane, the total pressure gradient being null. The P84 HF membranes were sealed in 1/8 in stainless steel tubing using epoxy resin glue (Fig. S2†). The

length between the seals was 13 cm, giving rise to an effective permeable area of 0.825 cm^2. Permeance values (mol m^{-2} s^{-1} Pa^{-1}) were calculated using the log-mean partial pressure difference along the HF once steady state was reached, whereas the separation selectivities corresponded to the ratios of permeances. In addition, the permeances of ZIF-8 and ZIF-93 *in situ* annealed membranes were measured at 100 °C after the annealing process.

XRD (X-ray diffraction) patterns were obtained using a D-Max Rigaku X-ray diffractometer (40 kV, 80 mA) with a Cu Kα (λ = 0.1542 nm) rotating anode from 4 to 36° (2θ) with a 0.025° s^{-1} step. TGA (thermo gravimetric analysis) were carried out with a Mettler Toledo TGA/DSC SF/755, oxidizing the samples in an air atmosphere from 25 to 850 °C at a rate of 10 °C min^{-1}. DSC (differential scanning calorimetry) analyses were made with a TA Instruments Q100 V9.9 Build 303 at a rate of 5 K min^{-1}. ATR-FTIR (attenuated total reflection-Fourier transform infrared spectroscopy) spectra were obtained using a Bruker Vertex 70, accumulating 40 scans from 4000 to 600 cm^{-1} with 4 cm^{-1} resolution. Cross-section SEM (scanning electron microscopy) images of the membranes were obtained using an FEI™ INSPECT-F and a FEI™ Nova200 with a cryo-transfer chamber, both operated at 10 kV. With the latter device, the MOF–polymer interface was brought to light by cryo-focused ion beam (FIB) technique, using Ga atoms for etching. EDS (energy dispersive spectroscopy) analyses of the main elements were obtained with an INCA PentaFET x3 (Oxford Instruments). AFM (atomic force microscopy) analyses were conducted at the inner of the HF supports using a VEECO Multimode 8 using the tapping mode and in ambient air conditions by using a silicon cantilever provided by Bruker. The average roughness parameters (R_a) were determined by the software and averaged from at least five 3 × 3 μm^2 areas starting from captured AFM images treated in a similar way. Finally, XPS (X-ray photoelectron spectroscopy) characterization was performed with a Kratos Axis Ultra spectrometer employing a monochromatic Al Kα (1486.6 eV) X-ray source at 10 mA and 15 kV and a power of 150 W. The samples were first evacuated at room temperature (pressures near 10^{-8} Torr were observed during surface analysis) and analyzed in 0.11 × 0.11 mm^2 areas at the same conditions. High resolution spectra of C 1s and N 1s regions were collected using a pass energy of 20 eV with 0.1 eV steps. Differential surface charging was minimized using a charge neutralizer system (flood gun). The binding energies were referenced to the C 1s (C–C peak at 284.9 eV) after background subtraction (Shirley baseline) using Casa software. To analyze the inner surface, P84 fibers were fixed by a double-side carbon tape and angle and lengthwise cut by means of small sharp scissors and tweezers.

Results and discussion

Effect of ZIF-8 HF membrane annealing on separation performance

The results obtained with the ZIF-8 membranes in the gas mixture separation tests are shown in Table 1 and Fig. 2, where the different MOF growths and thermal treatments (24 h-annealing, either in the vacuum oven or *in situ* in the permeation setup) applied and their influence on the final performance can be followed. An important enhancement in the gas separation selectivity was observed when a ZIF-8 growth took place on the surface of an as-synthetized P84 HF (D-type membrane). A selectivity of 43.5 in the H_2/CH_4 separation (20.4 in that of CO_2/CH_4) with a 1.5 × 10^{-8} mol m^{-2} s^{-1} Pa^{-1} H_2 permeance was measured, implying a molecular sieving transport through the microporosity of the polycrystalline MOF layer inside the HF. Methane molecules (0.38 nm kinetic diameter) were excluded from the ZIF-8 pore entrances (0.34 nm), that otherwise allowed the transport of smaller H_2 and CO_2 (0.29 and 0.33 nm, respectively). This MOF has been widely used as an adsorbent and molecular sieve in membrane studies including our previous works on growth on polysulfone supports.[39,46]

The D-type ZIF-8 membranes were thermally annealed in the vacuum oven (E-type membrane) and *in situ* during the permeation testing (G-type). The vacuum-annealed D-type membrane (E-type membrane) resulted in a lower H_2/CH_4 selectivity of 28.6 compared with the non-annealed membrane (D-type). On the contrary, G-type membrane resulted from the *in situ* annealed D-type membrane in a H_2/CH_4/Ar atmosphere. Its H_2 permeance remained almost constant (1.5 to 1.3 × 10^{-8} mol m^{-2} s^{-1} Pa^{-1}) with the applied treatment, while the H_2/CH_4 selectivity of the annealed membrane 66% increased (from 43.5 to 72.4) after the 24 h-heating up to 175 °C. Permeation data of the ZIF-8 *in situ* annealed P84 membrane (G-type) in the H_2/CH_4 separation at 35 and 100 °C are shown in Fig. S3:† a selectivity of 103 together with a H_2 permeance of 3.5 × 10^{-8} mol m^{-2} s^{-1} Pa^{-1} was achieved at 100 °C. In the CO_2/CH_4 mixture (see Table 1), CO_2 appears to have some preferential adsorption on the surface of the initial membrane that hinders after the *in situ* annealing treatment, so that the separation selectivity slightly decreases from 20.4 to 18.4.

An *in situ* annealed ZIF-8@P84 membrane (G-type) was also observed by SEM, showing a 1.3 ± 0.5 μm well-intergrown continuous MOF layer all along the P84 support (Fig. 3). When observing the interface in depth (etched with a Ga-beam), no apparent differences with non-annealed membranes were observed. EDS-mapping (Fig. 3d) showed the presence of Zn from the ZIF-8 confined in a thin layer that provided high methane exclusion in the gas mixture separation. The improvement in the membrane performance would then be related with some rearrangement of the polymer chains near the MOF crystals in the MOF–polymer interface, therefore increasing the MOF–polymer adherence and interaction and closing some existing gas bypass pathways. The presence of the MOF coating and MOF–polymer interpenetrated composite in the HF inner surface inhibits the creation of a dense layer of pure polymer, which would sharply decrease the gas permeance, as will be observed below. We can hypothesize that if the thermal annealing was carried out in the presence of air (E-type membrane, despite the 10 mbar vacuum atmosphere), the mechanism of formation of these new interactions together with the polymer rearrangement changes somehow in the presence of oxygen traces, and MOF–polymer adhesion worsens in comparison with an as-synthetized membrane. Therefore the

Table 1 Performance values at 35 °C of bare P84 HFs and ZIF-8@P84 HFs for H_2/CH_4 and CO_2/CH_4 mixture separation

		H_2 permeance			CO_2 permeance		
Description of the membrane		mol m^{-2} s^{-1} Pa^{-1}	GPU	H_2/CH_4 selectivity	mol m^{-2} s^{-1} Pa^{-1}	GPU	CO_2/CH_4 selectivity
A	Pure P84 HF	1.4×10^{-7}	429	4.9	5.2×10^{-8}	155	2.0
B	*In situ* annealed P84 HF	2.5×10^{-8}	73	36.9	8.7×10^{-9}	26	15.2
C	Vacuum annealed P84 HF	4.8×10^{-8}	142	11.6	1.1×10^{-8}	34	3.0
D	ZIF-8@P84 HF membrane	1.5×10^{-8}	46	43.5	4.7×10^{-9}	14	20.4
E	Vacuum annealed D membrane	9.9×10^{-9}	29	28.6	1.6×10^{-8}	4.7	5.0
F	ZIF-8@vaccum annealed P84 HF	5.9×10^{-8}	176	4.7	2.0×10^{-8}	59	1.7
G	*In situ* annealed D membrane	1.3×10^{-8}	39	72.4	2.8×10^{-9}	8.3	18.4

selectivity falls when the thermal treatment is completed (E-type membrane).

The *in situ* annealing process was monitored by a continuous measuring of H_2 and CH_4 permeances with time and temperature and depicted in Fig. 4a and b. The ZIF-8 membrane achieved its maxima H_2/CH_4 selectivity at temperatures around 100 °C, both in the heating and cooling stages. When cooling, the selectivity passed through a much higher maximum confirming the positive effect of the thermal annealing during the plateau at 175 °C. In general, selectivity maxima are obtained because of the favored CH_4 diffusion through the own MOF microporosity (and its intrinsic flexibility) and the polymeric chain mobility at high temperatures.

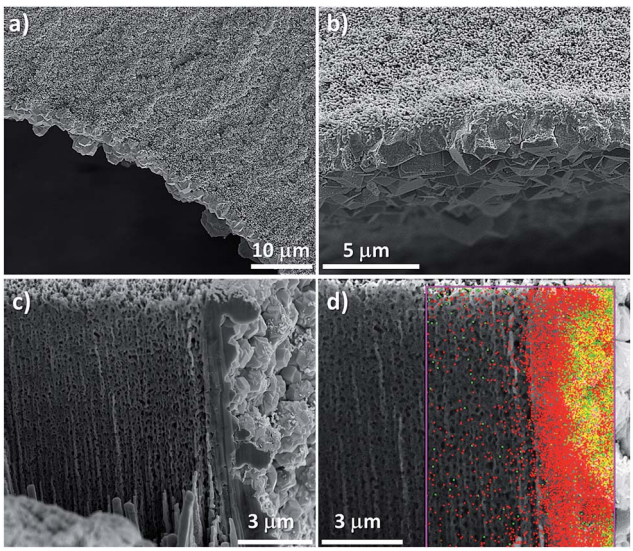

Fig. 3 SEM cross-section images of a G-type (*in situ* annealed) ZIF-8@P84 membrane (a and b). FIB-etched region showing the MOF–polymer interface (c), EDS mapping with Zn in red (d).

Effect of annealing on the pure P84 HF supports

An analogous maximum is observed (Fig. 4c and d) in the cooling stage of the *in situ* annealing of a pure P84 HF (B-type membrane in Fig. 2). When monitoring the annealing of the pure polymer, the induced changes (assumed to be related to the creation of new charge interactions, polymer chains relocation and then a free volume reduction, as previously reported for this kind of polymer)[19,23] led to a significant increase in the

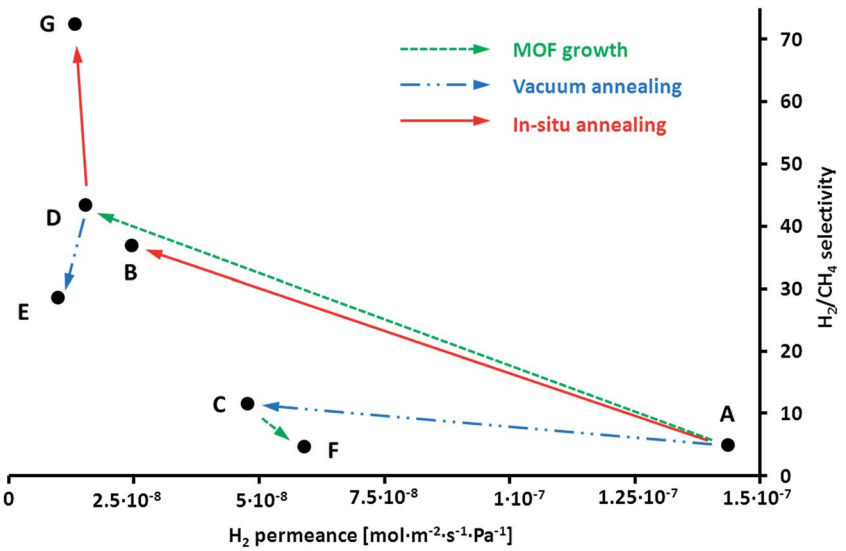

Fig. 2 Selectivity/permeance diagram for H_2/CH_4 mixture separation at 35 °C of bare P84 HFs and ZIF-8@P84 HFs.

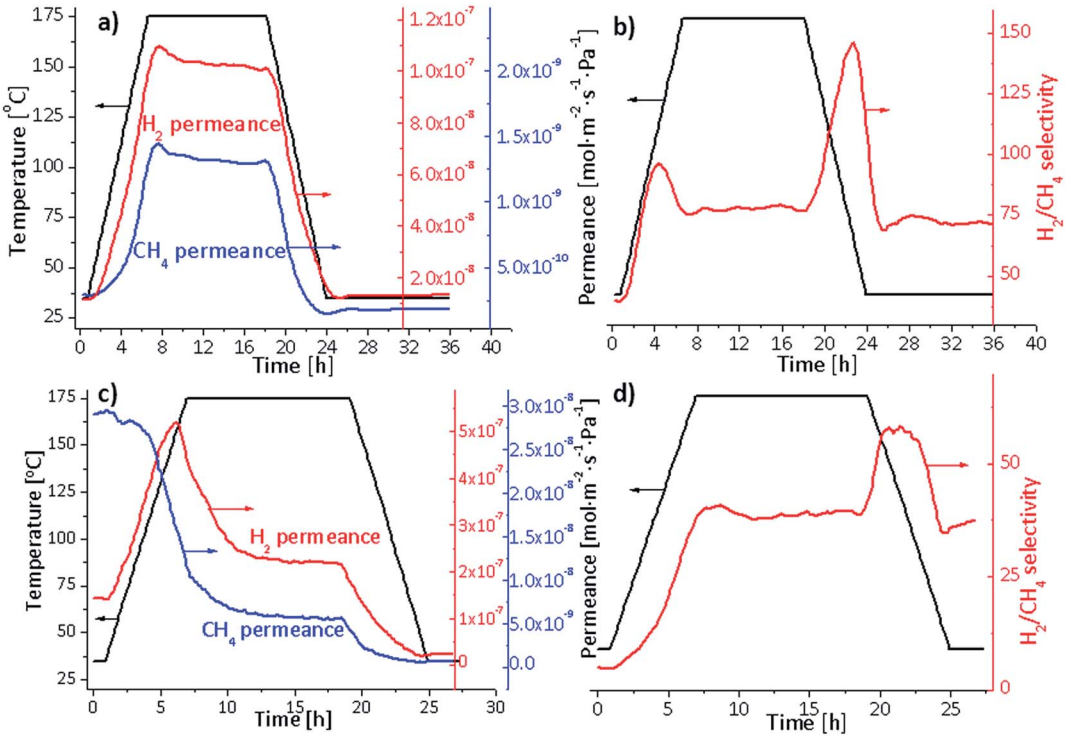

Fig. 4 H_2 and CH_4 permeances and mixture selectivity dependence with time during *in situ* thermal annealing. A D-type ZIF-8@P84 HF membrane was heated at 175 °C for 24 h with 6 h heating/cooling stages while separating a H_2/CH_4 gas mixture, resulting in a G-type membrane (a and b). The same procedure was applied to a pure P84 HF membrane (A-type), resulting in a B-type membrane (c and d).

separation selectivity together with a gas permeance decrease. The pure polymer membrane achieved its steady-state (annealed) from the seventh hour at the plateau at 175 °C, corresponding to a H_2/CH_4 selectivity of 36.9 when cooled at 35 °C with an almost 10-fold loss of H_2 permeance (2.5×10^{-8} mol m^{-2} s^{-1} Pa^{-1}, B-type membrane, Fig. 4c and d).

In any event, the bare P84 support (A) was annealed (either in vacuum or *in situ* during the permeation testing), its selectivity in the H_2/CH_4 separation increased, whereas the permeance sharply decreased. Pristine P84 HF supports (Table 1, point A) were not defect-free prepared and their porosity gave rise to permselective properties far from the intrinsic separation of P84 (CO_2/CH_4 and CO_2/N_2 selectivities up to 50 with 1–5 GPU CO_2 permeance)[13,47] but appropriate to be used as membrane supports. As observed in the ZIF-8 membrane performance, differences between both annealing treatments (in the case of membranes B and C, H_2 permeance decreased from 1.4×10^{-7} mol m^{-2} s^{-1} Pa^{-1} for membrane A to 2.5×10^{-8} and 4.8×10^{-8} mol m^{-2} s^{-1} Pa^{-1} after the *in situ* and vacuum treatments, respectively) might be explained by the different atmospheres: H_2/CH_4/Ar *versus* some remaining oxygen (air) despite the vacuum (10 mbar) applied.

Annealed P84 HF supports were then characterized. The images obtained from the bare and the annealed P84 supports reveal some densification in the polymeric HF,[19] although it can be said that it was not fully completed and some void fraction and open pores remained when observing both the inner and the outer support surfaces (Fig. 5). A denser-like polymeric layer (thinner than 2 μm) can barely be measured in both the vacuum and *in situ* annealed P84 fibers (Fig. 5b and c), which is intimately related to the reorganizing of the polymer chains and a decrease of the void fraction, which takes place from the internal surface and spreads to the bulk material,[48] and that causes a the decrease in the gas permeation of those samples (see Fig. 2, A-, B- and C-type membranes). This denser zone was not observed in the initial bare polymer (Fig. 5a).

Meanwhile no evidences of chemical bonding changes in the annealed P84 samples were found either when analyzed by FTIR or on its inner surface by XPS (see Fig. S4 and S5†). Carbon and nitrogen XPS spectra showed any shift in binding energies both in the vacuum and in the *in situ* 24 h annealed P84 fibers. However, the narrower and more intense peaks of the spectra compared with the pristine sample can be due to the rearrangement of the polymer chains leading to stiffening and reduced mobility. This approaching between the polymer species may enhance the size and shape molecule discrimination and the charge interactions between nearby groups.[18,26]

Moreover, a second glass transition temperature (T_g) was observed for the annealed HFs (361 °C, in addition to the T_g of the raw P84 HF at 322 °C, see Fig. S6†). This higher T_g suggests the rearrangement of part of the polymer in a more rigidified and dense form, caused by the thermal annealing applied.[48] The DSC curve of a MOF@P84 annealed membrane showed the absence of this second T_g, but some increasing in the T_g of the pristine polymer (334 *versus* 322 °C) indicating some disparity in the annealing process of the P84 HF when coated with MOF.

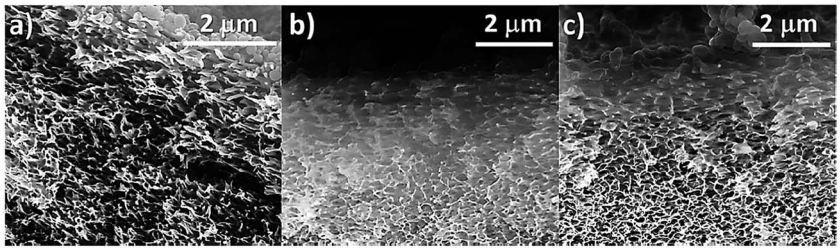

Fig. 5 SEM cross-section images of the raw P84 HF polymer (a), the *in situ* (b) and the vacuum (c) annealed P84 HFs, showing some densification and decreasing of the free volume near the surface.

Hence a great advance can be deduced: the *in situ* annealing of a ZIF-8 membrane growth on the inner surface of a P84 HF led to an important enhancement of its performance (separation selectivity) without any significant decrease inflicted on the H_2 permeance rate. Our hypothesis is that the layer-forming MOF crystals were involved in the reordering of the P84 chains and the creation of new intra- and intermolecular π-interactions between them, reducing the non-selective gas bypasses and increased the overall selectivity. Therefore the MOF layer reduced the densification of the polymer near the surface which would have led to a permeance decreasing,[49] generating a high permeable MOF–polymer composite region (see Fig. S7†). This behavior would confirm the strong affinity between the MOF and the co-polyimide P84, resulting in continuous membranes with a high degree of sturdiness and durability, jointly featuring the benefits of the polymers and the MOF organic moieties as previously described.

When a ZIF-8 synthesis was applied on the vacuum-annealed inner-surface of the P84 HF (F-type membrane), its final performance was far from that of a high-quality membrane. This procedure seemed virtually ineffective compared with a growth inside a raw non-annealed P84 HF (D-type). This behavior suggests some smoothing and increased stiffness of the polymer surface,[19] driven by the mobility and densification of the polymer chains, as observed above by SEM, and the possible creation of intermolecular charge-transfer complexes (CTCs, that may act as electrostatic charge sinks) during the pure polymer annealing. This would hinder an adequate ZIF-8 nucleation and subsequent anchoring during the synthesis and therefore inhibit the creation of a high quality continuous selective layer.[50] Besides, a significant inner-surface smoothing was observed after the vacuum annealing of a bare P84 support by AFM, with an averaged surface roughness (R_a) 23% decrease from 205 ± 14 nm (raw P84) to 167 ± 8 nm (annealed P84). Fig. 6 shows 3D inner-surface rendering of these P84 HF supports. This smoothing could be related with the subsequent poor MOF adhesion during the microfluidic synthesis (F-type membrane).

A low MOF content (5.0 wt% of ZIF-8 in the F-type membrane) was then calculated by TGA analyses, related with a worsened MOF-surface interaction as compared with the 14.2 wt% of ZIF-8 within the G-type membrane (see Fig. S8† showing its weight loss and weight loss rate curves) considering its residue at 850 °C as ZnO and comparing it with that of ZIF-8 powder (34.0 wt%). F-type membrane had its maximum degradation rate at an intermediate temperature of 592 °C while G-type degraded at maximum speed at 575 °C owing to the presence of Zn released from the MOF acting as catalysts in the polymer oxidation (bare P84 HF had its maximum at 615 °C). Hence, both the MOF content and separation performance of the membrane were worse if the annealing of the polymer was carried out before the MOF synthesis due to some surface smoothing and rigidification, which in turn prevented an optimum MOF–polymer interaction.

To conclude, it is worth mentioning that the outstanding performance enhancement was only attained when the polymer annealing was carried out with its inner-surface coated with ZIF-8 (G-type). The annealing effect itself on the bare HF (B-type) produced a similar (slightly worse) result than the growth of ZIF-8 on the same non-annealed support (D-type), but led to a large permeance drop and altered the support surface, as demonstrated by XPS, DSC, SEM and AFM, which makes the subsequent MOF growth non-effective.

Generalization for ZIF-93 membranes

The feasibility and repeatability of the procedure for the fabrication of MOF-supported membranes was proven with ZIF-93 (ZIF-93@P84). This MOF crystallizes in a wider structure (rho) than ZIF-8 (sod), with a pore size aperture of 0.36 nm.[42] Fig. S9† shows SEM images of an as-synthetized D′-type membrane cross-section with a continuous MOF layer of 2.6 ± 0.4 μm thickness strongly attached to the highly porous P84 support.

The ZIF-93@P84 membranes performed similarly to the ZIF-8 membranes, including their separation properties after annealing. The performance values in the H_2/CH_4 and CO_2/CH_4 mixture separations are shown in Fig. S10.† A H_2/CH_4 selectivity of 32.4 with a 3.9×10^{-9} mol m^{-2} s^{-1} Pa^{-1} H_2 permeance was obtained when ZIF-93 was grown inside the bare P84 HF (D′-type membrane), which enhanced its properties when *in situ* annealed at 175 °C. That is, a 101% increase in H_2/CH_4 selectivity of 65.0 with a slightly decreased H_2 permeance: 3.3×10^{-9} mol m^{-2} s^{-1} Pa^{-1} was achieved for the G′-type membrane. Neither the vacuum annealing nor the MOF growth on the annealed support (E′- and F′-type) had a positive effect on the final membrane, as was the case with ZIF-8.

The *in situ* annealing treatment monitoring (Fig. S11†) showed how the membrane changed during the annealing at 175 °C. Now the membrane keeps its gas permeance almost

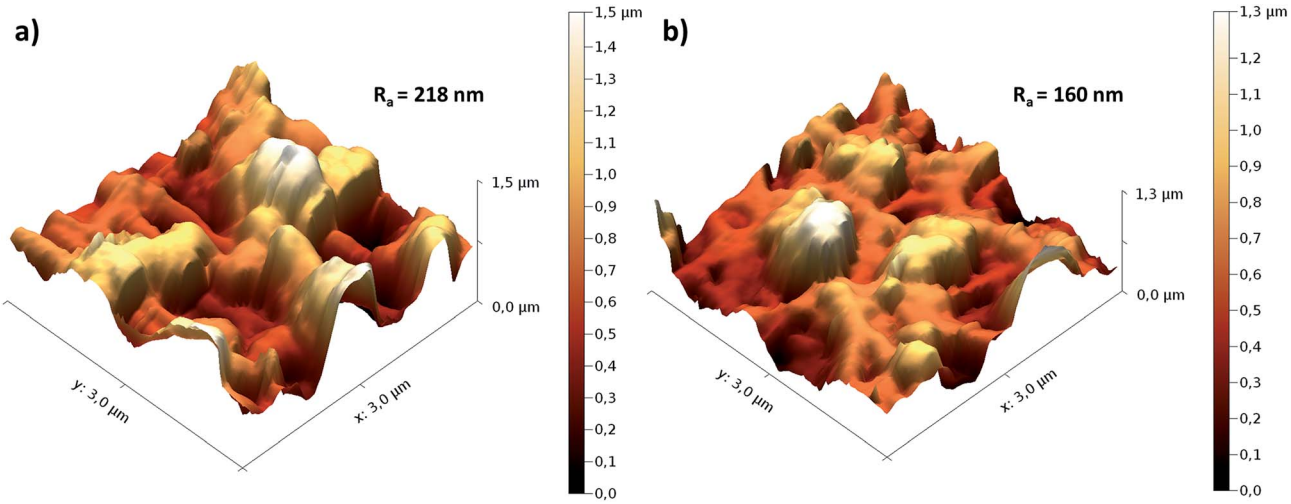

Fig. 6 AFM 3D surface rendering and averaged surface roughness (R_a) of the inner side of a raw (a) and a vacuum annealed (b) selected areas of the P84 hollow fiber supports.

constant at that temperature. The fact that both heating and cooling H_2/CH_4 selectivity maxima were almost the same for the ZIF-93 membrane suggests a faster annealing during the heating stage and in consequence a stabilization effect of the membrane that may be assigned to the positive MOF–polymer synergy. In agreement with the previous discussion concerning the annealing of bare P84 and ZIF-8 HFs, this suggests a stronger affinity with polyimide for ZIF-93 than for ZIF-8 related to the functional pending aldehyde group present in ZIF-93. The annealed ZIF-93 membrane was then measured at 100 °C, giving rise to a 101.3 H_2/CH_4 selectivity with a temperature-activated H_2 permeance of 1.0×10^{-8} mol m^{-2} s^{-1} Pa^{-1}.

Regarding our best value of CO_2/CH_4 selectivity of 19.6, this is not far from the simulated value of 26.7 given by Ray *et al.*[42] Moreover, these authors predicted that ZIF-93 was the best performing rho-type ZIF in this separation of a series including ZIF-25, −71, −93, −96, and −97.

In any event, the results were better for ZIF-8@P84 than for ZIF-93@P84 membranes, implying that several factors may contribute to the optimum performance of the membranes: the ZIF pore size and surface chemistry and the different annealing behavior. As shown in Fig. 7, a better separation performance (simultaneous permeance and selectivity) was obtained with ZIF-8 than with ZIF-93 in both H_2/CH_4 and CO_2/CH_4 separations. This is related with the smaller pore size (sod *versus* rho with respective 6- and 8-ring windows and hence an increased size-exclusion effect for CH_4) and the thinner layer observed (1.3 for ZIF-8 *versus* 2.6 µm for ZIF-93, giving rise to a 3.7 times greater permeance).

Fig. 7 shows the gas H_2, CO_2 and CH_4 permeation rates at 35 °C in the *in situ* annealed ZIF-8 (G-type) and ZIF-93 (G′-type) membranes *versus* the inverse of the square root of the molecular weight of the corresponding molecule. The linear proportion of H_2 (0.29 nm kinetic diameter) and CO_2 (0.33 nm) permeances in both membranes is related with a free pass of the molecules through the microporous structure of the MOF (pore apertures of 0.34 nm in ZIF-8 and 0.36 nm in ZIF-93), while the exclusion of the larger CH_4 (0.38 nm) justifies its lack of linearity. No significant preferential CO_2 adsorption is inferred from these results, since the CH_4 permeance was practically the same in both H_2/CH_4 and CO_2/CH_4 separations. The CH_4 permeance in Fig. 7 was averaged from both separations.

Comparison with literature

A bibliographic comparison of our ZIF-8@P84 and ZIF-93@P84 membranes in the H_2/CH_4 separation performance is presented in Fig. 8 (see detailed data in Table S3†). They were compared with previously reported data on MOF supported HF membranes,[35,36,39] (with high permeances and H_2/CH_4 selectivities below 10), pure polyimide HFs[51–53] and some CMSMs

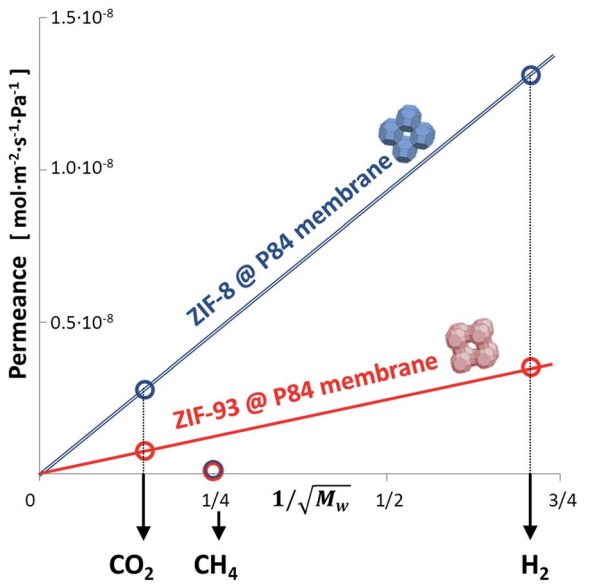

Fig. 7 Gas permeances of the *in situ* annealed ZIF-8@P84 and ZIF-93@P84 HF membranes at 35 °C with respect to the inverse of the square root of the molecular weight of the gas molecule.

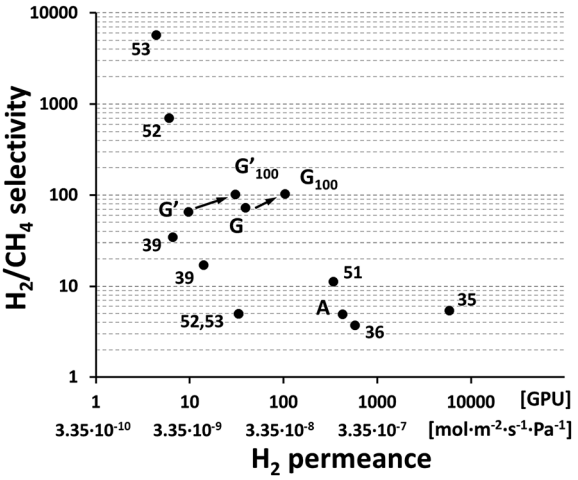

Fig. 8 H_2/CH_4 performance comparison of the ZIF-8@P84 and ZIF-93@P84 HF membranes (measured at 35 and 100 °C, see Fig. 2 and S3†) with the performances of previously reported HF membranes: those of MOFs,[35,36,39] pure polyimide[51–53] and some CMSMs[52,53] derived from them. See ESI for additional information in Table S3.† All data were obtained in the 20–60 °C temperature range with the exception of G_{100} and G'_{100}.

derived from them[52,53] (carbon molecular sieve membranes, with low H_2 permeances but exceptionally high selectivities).

CMSMs are an alternative strategy to increase the membrane performance based on the pyrolysis of a precursor polymeric membrane in a controlled atmosphere (generally a vacuum or inert one). This kind of membranes has been proven to be very competitive in gas separation processes.[51,52] Also, porous HF shaped polymeric membranes, even with some filler content, have been used as precursors for these CMSMs.[54,55]

The inner-supported MOF membranes synthesized with our microfluidic approach in this work (G and G′-type membranes), submitted to *in situ* annealing, show H_2/CH_4 selectivities in the 100 range with intermediate permeances (40–60 GPU H_2), representing a well balanced performance.

Conclusions

Highly selective MOF (ZIFs ZIF-8 and ZIF-93) supported membranes for H_2 and CO_2 separation from CH_4 have been synthesized inside P84 (ZIF@P84) hollow fibers by microfluidics. These ZIFs, and MOFs in general, have organic moieties which make them highly compatible with polymers, combining the advantages of both materials in a single membrane with attractive separation properties.

The affinity between the polymer support and MOF was enhanced when the ZIF@P84 hollow fiber membrane was annealed *in situ* at a temperature (175 °C) below the glass transition temperature. This procedure improved the interaction (*i.e.* the MOF–polymer adherence) *via* a synergetic rearrangement of the polymer chains in the presence of the ZIF particles forming continuous layers (as the characterization by SEM, XPS and DSC suggested), leading to an increase in the H_2/CH_4 separation selectivity without any permeation rate loss. The MOF growth and subsequent separation performance of the membranes only improved if the thermal annealing process was carried out after the MOF synthesis due to the better MOF–polymer interaction achieved. An annealing of the polymeric support before the synthesis of the MOF smoothed the support surface (as seen by SEM and AFM) giving rise to a poor MOF–polymer interaction.

Acknowledgements

Financial support (MAT2013-40556-R) from the Spanish MINECO, the Aragón Government (DGA) and the European Social Fund is gratefully acknowledged. We also acknowledge the use of the Servicio General de Apoyo a la Investigación-SAI (Universidad de Zaragoza). F. C.-B. thanks the DGA fellowship. All the microscopy work was done in the Laboratorio de Microscopías Avanzadas at the Instituto de Nanociencia de Aragón (LMA-INA). The authors acknowledge the LMA-INA for offering access to their instruments and expertise.

Notes and references

1 R. P. Lively, M. E. Dose, L. Xu, J. T. Vaughn, J. R. Johnson, J. A. Thompson, K. Zhang, M. E. Lydon, J. S. Lee, L. Liu, Z. Hu, O. Karvan, M. J. Realff and W. J. Koros, *J. Membr. Sci.*, 2012, **423–424**, 302–313.
2 S. H. Choi, A. Brunetti, E. Drioli and G. Barbieri, *Sep. Sci. Technol.*, 2011, **46**, 1–13.
3 Y. Yampolskii, *Macromolecules*, 2012, **45**, 3298–3311.
4 P. Bernardo, E. Drioli and G. Golemme, *Ind. Eng. Chem. Res.*, 2009, **48**, 4638–4663.
5 C. Y. Feng, K. C. Khulbe, T. Matsuura and A. F. Ismail, *Sep. Purif. Technol.*, 2013, **111**, 43–71.
6 M. Rafat, D. De, K. C. Khulbe, T. Nguyen and T. Matsuura, *J. Appl. Polym. Sci.*, 2006, **101**, 4386–4400.
7 R. Mukherjee and S. De, *J. Membr. Sci.*, 2014, **466**, 281–292.
8 J. J. Krol, M. Boerrigter and G. H. Koops, *J. Membr. Sci.*, 2001, **184**, 275–286.
9 L. Liu, E. S. Sanders, S. S. Kulkarni, D. J. Hasse and W. J. Koros, *J. Membr. Sci.*, 2014, **465**, 49–55.
10 Y. Zhang, I. H. Musselman, J. P. Ferraris and K. J. Balkus, *J. Membr. Sci.*, 2008, **313**, 170–181.
11 Y. Dai, J. R. Johnson, O. Karvan, D. S. Sholl and W. J. Koros, *J. Membr. Sci.*, 2012, **401–402**, 76–82.
12 V. Galstyan, E. Comini, C. Baratto, A. Ponzoni, E. Bontempi, M. Brisotto, G. Faglia and G. Sberveglieri, *CrystEngComm*, 2013, **15**, 2881–2887.
13 J. N. Barsema, G. C. Kapantaidakis, N. F. A. van der Vegt, G. H. Koops and M. Wessling, *J. Membr. Sci.*, 2003, **216**, 195–205.
14 S. Sorribas, P. Gorgojo, C. Tellez, J. Coronas and A. G. Livingston, *J. Am. Chem. Soc.*, 2013, **135**, 15201–15208.
15 R. X. Liu, X. Y. Qiao and T. S. Chung, *J. Membr. Sci.*, 2007, **294**, 103–114.
16 D. Hua, Y. K. Ong, Y. Wang, T. Yang and T. S. Chung, *J. Membr. Sci.*, 2014, **453**, 155–167.

17 C. Ba, J. Langer and J. Economy, *J. Membr. Sci.*, 2009, **327**, 49–58.
18 K. Vanherck, P. Vandezande, S. O. Aldea and I. F. J. Vankelecom, *J. Membr. Sci.*, 2008, **320**, 468–476.
19 X. Qiao, T. S. Chung and K. P. Pramoda, *J. Membr. Sci.*, 2005, **264**, 176–189.
20 W. Qiu, C.-C. Chen, L. Xu, L. Cui, D. R. Paul and W. J. Koros, *Macromolecules*, 2011, **44**, 6046–6056.
21 M. Askari and T. S. Chung, *J. Membr. Sci.*, 2013, **444**, 173–183.
22 S. Shahid and K. Nijmeijer, *J. Membr. Sci.*, 2014, **470**, 166–177.
23 K. Vanherck, G. Koeckelberghs and I. F. J. Vankelecom, *Prog. Polym. Sci.*, 2013, **38**, 874–896.
24 H. Kawakami, M. Mikawa and S. Nagaoka, *J. Membr. Sci.*, 1996, **118**, 223–230.
25 Y. Shen and A. C. Lua, *J. Appl. Polym. Sci.*, 2010, **116**, 2906–2912.
26 Y. Xiao, B. T. Low, S. S. Hosseini, T. S. Chung and D. R. Paul, *Prog. Polym. Sci.*, 2009, **34**, 561–580.
27 A. Bos, I. G. M. Pünt, M. Wessling and H. Strathmann, *Sep. Purif. Technol.*, 1998, **14**, 27–39.
28 S. Japip, H. Wang, Y. Xiao and T. S. Chung, *J. Membr. Sci.*, 2014, **467**, 162–174.
29 T. Yang, Y. Xiao and T. S. Chung, *Energy Environ. Sci.*, 2011, **4**, 4171.
30 D. Nagaraju, D. G. Bhagat, R. Banerjee and U. K. Kharul, *J. Mater. Chem. A*, 2013, **1**, 8828–8835.
31 K. Díaz, L. Garrido, M. López-González, L. F. del Castillo and E. Riande, *Macromolecules*, 2010, **43**, 316–325.
32 Y. Peng, Y. Li, Y. Ban, H. Jin, W. Jiao, X. Liu and W. Yang, *Science*, 2014, **346**, 1356–1359.
33 R. Jin, Z. Bian, J. Li, M. Ding and L. Gao, *Dalton Trans.*, 2013, **42**, 3936–3940.
34 B. P. Biswal, A. Bhaskar, R. Banerjee and U. K. Kharul, *Nanoscale*, 2015, **7**, 7291–7298.
35 Y. Mao, J. Li, W. Cao, Y. Ying, L. Sun and X. Peng, *ACS Appl. Mater. Interfaces*, 2014, **6**, 4473–4479.
36 A. J. Brown, J. R. Johnson, M. E. Lydon, W. J. Koros, C. W. Jones and S. Nair, *Angew. Chem., Int. Ed.*, 2012, **51**, 10615–10618.
37 W. Li, P. Su, G. Zhang, C. Shen and Q. Meng, *J. Membr. Sci.*, 2015, **495**, 384–391.
38 W. Li, Q. Meng, C. Zhang and G. Zhang, *Chem.–Eur. J.*, 2015, **21**, 7224–7230.
39 F. Cacho-Bailo, S. Catalán-Aguirre, M. Etxeberría-Benavides, O. Karvan, V. Sebastian, C. Téllez and J. Coronas, *J. Membr. Sci.*, 2015, **476**, 277–285.
40 A. J. Brown, N. A. Brunelli, K. Eum, F. Rashidi, J. R. Johnson, W. J. Koros, C. W. Jones and S. Nair, *Science*, 2014, **345**, 72–75.
41 W. Morris, N. He, K. G. Ray, P. Klonowski, H. Furukawa, I. N. Daniels, Y. A. Houndonougbo, M. Asta, O. M. Yaghi and B. B. Laird, *J. Phys. Chem. C*, 2012, **116**, 24084–24090.
42 K. G. Ray, D. L. Olmsted, J. M. R. Burton, Y. Houndonougbo, B. B. Laird and M. Asta, *Chem. Mater.*, 2014, **26**, 3976–3985.
43 W. Morris, B. Leung, H. Furukawa, O. K. Yaghi, N. He, H. Hayashi, Y. Houndonougbo, M. Asta, B. B. Laird and O. M. Yaghi, *J. Am. Chem. Soc.*, 2010, **132**, 11006–11008.
44 F. Cacho-Bailo, G. Caro, M. Etxeberria, O. Karvan, C. Tellez and J. Coronas, *Chem. Commun.*, 2015, **51**, 11283–11285.
45 D. T. Clausi and W. J. Koros, *J. Membr. Sci.*, 2000, **167**, 79–89.
46 F. Cacho-Bailo, B. Seoane, C. Téllez and J. Coronas, *J. Membr. Sci.*, 2014, **464**, 119–126.
47 P. S. Tin, T. S. Chung, Y. Liu and R. Wang, *Carbon*, 2004, **42**, 3123–3131.
48 L. Li, D. Zhou, D. Huang and G. Xue, *Macromolecules*, 2014, **47**, 297–303.
49 A. F. Ismail, R. A. Rahim and W. A. Rahman, *Sep. Purif. Technol.*, 2008, **63**, 200–206.
50 M. Navarro, B. Seoane, E. Mateo, R. Lahoz, G. F. de la Fuente and J. Coronas, *J. Mater. Chem. A*, 2014, **2**, 11177–11184.
51 E. P. Favvas, G. C. Kapantaidakis, J. W. Nolan, A. C. Mitropoulos and N. K. Kanellopoulos, *J. Mater. Process. Technol.*, 2007, **186**, 102–110.
52 E. P. Favvas, E. P. Kouvelos, G. E. Romanos, G. I. Pilatos, A. C. Mitropoulos and N. K. Kanellopoulos, *J. Porous Mater.*, 2008, **15**, 625–633.
53 E. P. Favvas, N. S. Heliopoulos, S. K. Papageorgiou, A. C. Mitropoulos, G. C. Kapantaidakis and N. K. Kanellopoulos, *Sep. Purif. Technol.*, 2015, **142**, 176–181.
54 Y. Li and T. S. Chung, *Microporous Mesoporous Mater.*, 2008, **113**, 315–324.
55 A. C. Lua and Y. Shen, *Chem. Eng. J.*, 2013, **220**, 441–451.